Spin excitation spectrum in a magnetic nanodot with continuous transitions between the vortex, Bloch-type skyrmion, and Néel-type skyrmion states

M. Mruczkiewicz,[1,*] M. Krawczyk,[2,†] and K. Y. Guslienko[3,4,‡]

[1]*Institute of Electrical Engineering, Slovak Academy of Sciences, Dubravska cesta 9, 841 04 Bratislava, Slovakia*

[2]*Faculty of Physics, Adam Mickiewicz University in Poznan, Umultowska 85, Poznań, 61-614, Poland*

[3]*Departamento de Fisica de Materiales, Universidad del Pais Vasco, UPV/EHU, 20018 San Sebastian, Spain*

[4]*IKERBASQUE, the Basque Foundation for Science, 48013 Bilbao, Spain*

(Received 11 October 2016; revised manuscript received 21 January 2017; published 13 March 2017)

We study spin-wave excitations in a circular ferromagnetic nanodot in different inhomogeneous, topologically nontrivial magnetization states, specifically, vortex and skyrmion states. Gradual change in the strength of the out-of-plane magnetic anisotropy and the Dzyaloshinskii-Moriya exchange interaction leads to continuous phase transitions between different stable magnetic configurations and allows for mapping of dynamic spin modes in and between the vortex, Bloch-type skyrmion, and Néel-type skyrmion states. Our study elucidates the connections between gyrotropic modes, azimuthal spin waves, and breathing modes in these various stable magnetization states and helps us to understand the rich spin excitation spectrum on the skyrmion background.

DOI: 10.1103/PhysRevB.95.094414

I. INTRODUCTION

Theory of two-dimensional (2D) magnetic topological solitons was developed in the 1980s, see Ref. [1] and references therein. The first kind of the topological solitons, magnetic vortex stabilized in flat soft magnetic particles (dots), was discovered in 2000 by Shinjo *et al.* [2]. The spin excitation spectrum over the vortex ground state was actively studied during the last decade and is now well established [3–6]. The classification of the vortex excitations on high frequency spin waves (SWs) and low frequency gyrotropic modes based on the mode symmetry and number of nodes of the dynamical magnetization profiles along the radial and azimuthal directions has been suggested. The vortex spin excitations are interesting from a physical point of view but also have important potential applications, for instance, for understanding of the switching of the vortex core polarization [7,8], an effect that might find an application in novel magnetic logic or memory devices [9].

2D hexagonal lattices of magnetic skyrmions (another kind of the topological solitons) were found in 2009 in thin films of some compounds with B20 cubical crystal structure without an inversion center (like MnSi, FeGe, etc.) and in some multiferroics (Cu_2SeO_3, etc.) at low temperatures. These skyrmion lattices are stabilized due to the antisymmetric Dzyaloshinskii-Moriya exchange interaction (DMI). Recently existence of the Néel skyrmions in ultrathin films/dots was experimentally confirmed for large enough interface DMI strength and $Q > 1$ (the Q-factor is defined as $Q = \frac{2K_u}{\mu_0 M_s^2}$) [10–12]. The Bloch skyrmions at $Q < 1$ were observed in CoB/Pt multilayer dots [13]. The spin excitation spectra of the skyrmion lattices were simulated [14] and measured by broadband ferromagnetic resonance [15,16]. Very recently the single skyrmions stabilized in ultrathin magnetic films and dots by an interface induced DMI were discovered using x-ray imaging [10–12]. Such individual skyrmions attracted attention due to their existence at room temperature, small (zero) magnetic field stability, and high mobility in response to spin polarized current [17]. The study of spin dynamics in the skyrmion state in restricted geometry (magnetic dots, stripes, etc.) is equally important, however, it is still in the beginning stage. The theory of the magnetic topological soliton dynamics developed so far, concerns so called precession solitons in infinite 2D systems (thin magnetic films). Typically the Belavin-Polyakov (no magnetic anisotropy) solitons [18] and the precessional solitons in uniaxial "easy" axis ferromagnets [19] were considered. The need to consider precession of the magnetic solitons appeared due to the problem with the soliton stability in the absence of the high-order exchange or Dzyaloshinskii-Moriya exchange interaction. The solitons were made conditionally stable fixing the number of bounded magnons [1]. The situation with magnetic dots/stripes is different: the topological soliton can be stabilized either by the DMI (bulk or interface) or magnetostatic interactions at some finite value of the uniaxial magnetic anisotropy. There are zero-frequency spin excitation modes for the topological solitons in infinite films (radially symmetric breathing mode and azimuthal translation mode) related to a degeneracy of the soliton ground state and several finite frequency modes localized near the soliton center. Nonzero-frequency modes are expected for the solitons in magnetic dots because the soliton energy depends on the soliton position and soliton radius due to existence of the sample edges. Even though several papers have been already published on the magnetic skyrmion dynamical excitations in restricted geometry [20–24], the consensus regarding the classification of the spin eigenmodes over the skyrmion background in nanodots has not been reached so far. Also a transition between the dynamical vortex and skyrmion modes has not been explored. This leaves many questions unanswered, in particular, whether the spin excitation modes corresponding to the two azimuthal SWs existing over a vortex state with clockwise (CW) and counterclockwise (CCW) sense of propagation can be found in the skyrmion states.

An analytic approach to the magnetic skyrmion dynamics in restricted geometry is related to some model assumptions and simplifications which sometimes are difficult to justify for

*m.mru@amu.edu.pl

†krawczyk@amu.edu.pl

‡kostyantyn.gusliyenko@ehu.eus

real systems. For instance, the ideas developed for description of the magnetic bubble domain dynamics in infinite films were exploited. The skyrmion dynamics in circular dots was considered assuming that all skyrmion excitation modes can be described as oscillation of the circular domain wall shape [25] or that the radial domain wall is very thin (the skyrmion radius is essentially larger than the domain wall width) [22].

In this paper we consider spin excitation spectra on the magnetic soliton background in thin circular dots with effective easy plane anisotropy by using micromagnetic simulations. To do that we identify a set of parameters that allows for the continuous phase transitions (preserving continuity of the magnetization components) [26,27] in transformations between various magnetic soliton stable states, i.e., vortex, Bloch-like skyrmion, and Néel-like skyrmion (see Fig. 1). With this we are able to show a continuous mapping of the spin eigenmodes between different inhomogeneous magnetization configurations and understand the relation between the excitation modes in different soliton stable states of the nanodots. The results enable us to classify the spin eigenmodes in the Bloch-like skyrmion and Néel-like skyrmion states and finally to demonstrate existence of the azimuthally symmetric CW and CCW spin-wave excitations in these skyrmion state dots.

II. MODEL

The physical system we consider is a circular ferromagnetic dot of the thickness t and radius R. To find the dot spin excitation spectrum the finite difference time domain (FDTD) micromagnetic simulations were performed using mumax^3 code [28]. We start from the Landau-Lifshitz-Gilbert equation of magnetization $\mathbf{M}$ motion with the Gilbert damping parameter in which the magnetization time derivative $\frac{\partial \mathbf{M}(\mathbf{r},t)}{\partial t}$ is defined as the torque τ, and equal to

$$\tau = \gamma \frac{1}{1+\alpha^2}\{\mathbf{M} \times \mathbf{B}_{\text{eff}} + \alpha[\mathbf{M} \times (\mathbf{M} \times \mathbf{B}_{\text{eff}})]\}, \quad (1)$$

where γ is the gyromagnetic ratio, α is a dimensionless damping parameter, and $\mathbf{B}_{\text{eff}}$ is the effective magnetic field, which includes the external magnetic field $\mathbf{B}_{\text{ext}}$, the magnetostatic demagnetizing field $\mathbf{B}_{\text{demag}}$, the isotropic Heisenberg exchange field $\mathbf{B}_{\text{exch}}$ (the parameter A_{exch}), the Dzyaloshinskii-Moriya exchange field $\mathbf{B}_{\text{DM}}$, and the uniaxial magnetocrystalline anisotropy field $\mathbf{B}_{\text{anis}}$ (the anisotropy constant K_u):

$$\mathbf{B}_{\text{eff}} = \mathbf{B}_{\text{ext}} + \mathbf{B}_{\text{demag}} + \mathbf{B}_{\text{exch}} + \mathbf{B}_{\text{DM}} + \mathbf{B}_{\text{anis}}. \quad (2)$$

The skyrmions are stabilized in the dot due to an interplay of the isotropic exchange, DMI, uniaxial out-of-plane magnetic anisotropy, and magnetostatic energies assuming zero bias magnetic field. The DMI is implemented as an effective field according to [29]

$$\boldsymbol{B}_{\text{DM}} = \frac{2D}{M_s}\left(\frac{\partial m_z}{\partial x}, \frac{\partial m_z}{\partial y}, -\frac{\partial m_x}{\partial x} - \frac{\partial m_y}{\partial y}\right) \quad (3)$$

that give rise to the magnetic energy density

$$\varepsilon = D[m_z(\nabla \cdot \boldsymbol{m}) - (\boldsymbol{m} \cdot \nabla)m_z], \quad (4)$$

where $\boldsymbol{m} = \boldsymbol{M}/M_s$ is the reduced magnetization vector, M_s is the saturation magnetization, and D is the Dzyaloshinskii-Moriya interface exchange interaction constant.

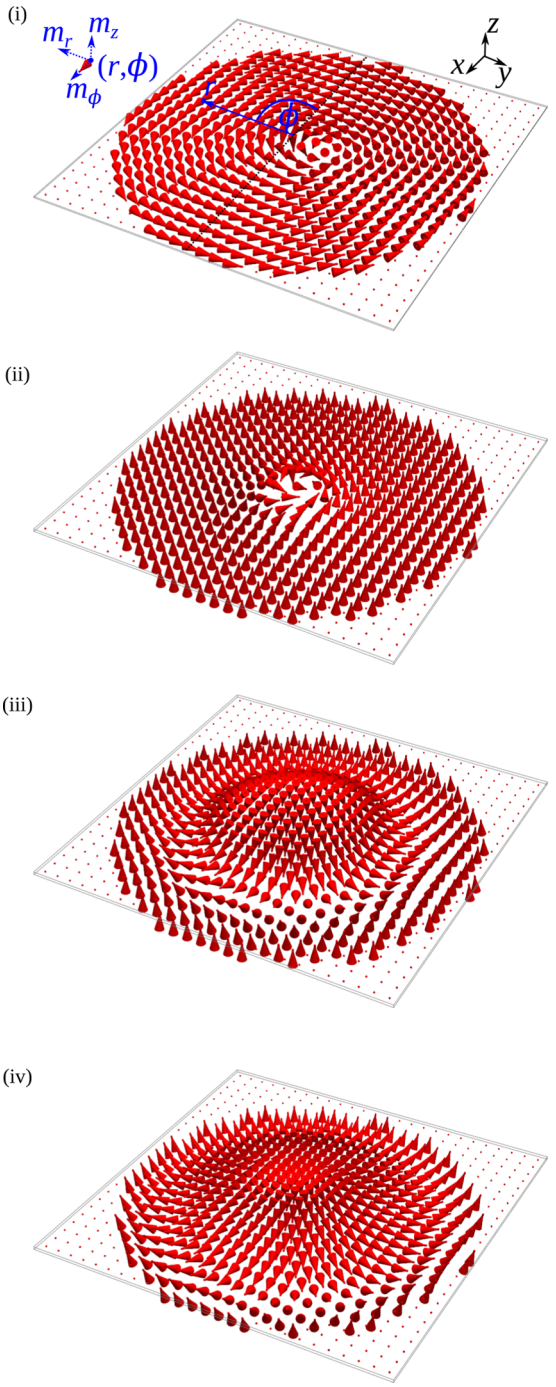

FIG. 1. The four topologically nontrivial magnetization configurations of the circular ferromagnetic dot investigated in the paper: (i) vortex, (ii) Bloch-like skyrmion, (iii) Néel-like skyrmion with strong perpendicular magnetic anisotropy (large value of the quality factor $Q = \frac{2K_u}{\mu_0 M_s^2}$), and (iv) Néel-like skyrmion with small value of Q.

The simulations consisted of the following steps. The initial state was assumed in the form of the Bloch skyrmion (Fig. 1). This state was relaxed to the lowest local minimum energy state and transformed during relaxation process into vortex, Bloch skyrmion, or Néel skyrmion state, depending on the chosen parameters (K_u, D). In the majority of the cases, the initial Bloch-like skyrmion state relaxes to the ground state (as

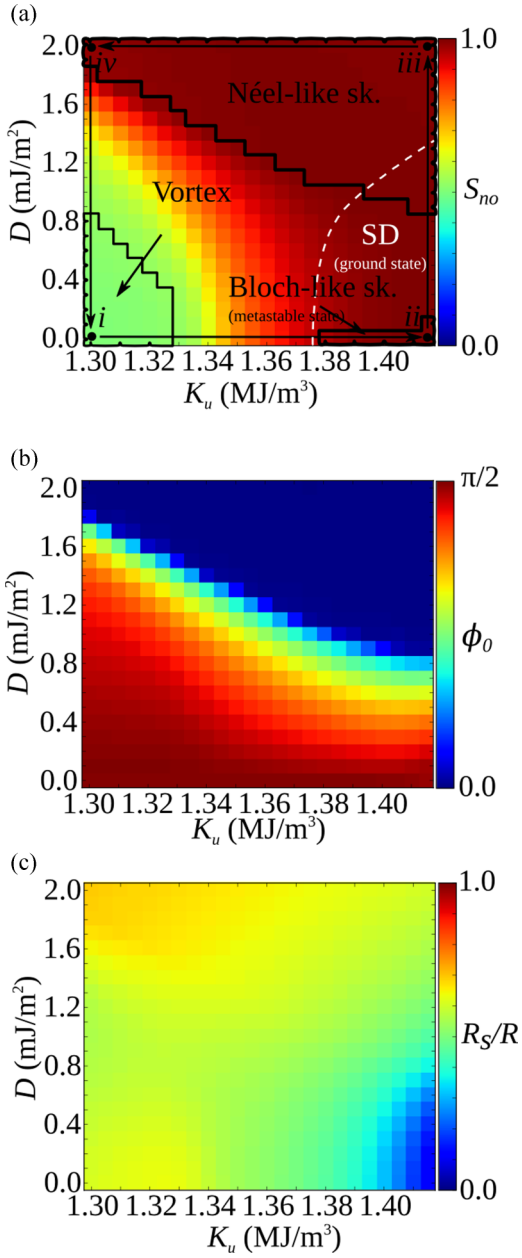

FIG. 2. The properties of the static configuration of the magnetic topological soliton in the isolated circular dot as a function of the parameters D and K_u: (a) skyrmion number $S_{\rm no}$, (b) skyrmion phase Φ_0, and (c) skyrmion size R_s/R. The points (i)–(iv) corresponding to magnetic configuration of Fig. 1 are shown in (a). The arrows indicate the path along which the resonance frequencies are simulated in Fig. 3. The black line in (a) indicates the area of the vortex, Bloch-like, and Néel-like skyrmion stability. The white dashed line indicates the region where a SD state was found with the energy lower than the magnetic soliton energies. The dot radius R is 125 nm and thickness is 1.4 nm.

compared with other initial states: vortex, Néel-like skyrmion, single domain, and random magnetization). The region where the Bloch-like skyrmion did not relax to the ground state was indicated by the white dashed line in Fig. 2(a) and a single domain (SD) state was used as an initial state to obtain the ground state.

Then, the stable magnetization configurations were excited with a uniform low amplitude variable magnetic field having a time dependence represented by sinc function with the cut-off frequency $f_{\rm max} = 10$ GHz [30]. Such low value of the cut-off frequency was chosen because we were interested to map the low frequency part of the dot spin excitation spectra related to the different dot inhomogeneous magnetization states. We used in-plane and out-of-plane orientation of the magnetic microwave field to excite the spin modes of different symmetry. The space and time dependent magnetization components acquired after the field excitation were then transformed to the frequency domain (Fourier transform [31]) to obtain the resonance frequencies of spin modes and spatial distribution of the dynamical components of the selected eigenoscillations of the magnetization vector $\boldsymbol{m}$ [24].

Throughout the paper we use the following material parameters of an ultrathin magnetic circular dot of the radius $R = 125$ nm and thickness $t = 1.4$ nm: saturation magnetization $M_s = 1.5 \times 10^6$ A/m, exchange stiffness constant $A_{\rm exch} = 3.1 \times 10^{-11}$ J/m, DMI constant $D = 0$–2×10^{-3} J/m^2, and out-of-plane magnetic anisotropy constant $K_u = 1.30 \times 10^6$–1.415×10^6 J/m^3. This set of parameters corresponds to the ultrathin layers of CoFeB-MgO [32]. These nanostructures have been considered as feasible to support the ground state vortex and Néel-like skyrmions. In addition, the electric field pulses were presented there as a process of nucleating the skyrmions. The material quality factor $Q = \frac{2K_u}{\mu_0 M_s^2}$ varies from 0.92 to 1.0. The assumed value of the Gilbert damping parameter taken into account in the FDTD simulations is $\alpha = 0.01$. It is close to the damping value of a ultrathin CoFeB film [33,34].

In order to show the continuous transitions between the vortex, Bloch-type skyrmion, and Néel-type skyrmion states we limit our investigation to one single sample with different DMI and magnetic anisotropy constants. The study of influence of other material or geometry parameters (including size of the dots) on the magnetization configuration stabilization and dynamics were partially presented elsewhere and are out of the scope of this study [3,20,23,35].

III. RESULTS AND DISCUSSION

The simulated static soliton stable configurations in the isolated circular dot shown in Fig. 2(a) are classified by using the skyrmion number (topological charge) [36]

$$S_{\rm no} = \frac{1}{4\pi} \int\int \boldsymbol{m} \cdot \left(\frac{\partial \boldsymbol{m}}{\partial x} \times \frac{\partial \boldsymbol{m}}{\partial y} \right) dx dy. \qquad (5)$$

The topological charge has the characteristic value of 0.5 for the vortex state and 1 for the skyrmion states. However, $S_{\rm no}$ is not exactly equal to 1 for a magnetic skyrmion in restricted geometry. It is shown that the topological charge $S_{\rm no}$ is a continuous function when the magnetic anisotropy or DMI values are changed in the range of interest defined in the previous section, see Fig. 2(a). The smooth transition is present from complete vortex (i) to complete Bloch-like (ii) or to Néel-like skyrmion (iii) and (iv) (these magnetization configurations are visualized in Fig. 1) with an increase of the magnetic anisotropy or DMI value. The solitons presented in the phase diagram are in ground state when in vortex or

Néel-like skyrmion configuration. The Bloch-like skyrmion is stabilized at high values of the anisotropy constant and $D \approx 0$. However, it is a metastable state. In Fig. 2 (a), the white dashed line indicates the region where SD state was found with the magnetic energy lower than the soliton energies. Even though the investigated Bloch-like skyrmion is a metastable state, the current, varying an out-of-plane bias magnetic field, picosecond magnetic field pulse, or electric field, could be used for its nucleation [17,32,37]. The Bloch-like skyrmion metastable state is considered in our simulations in order to have continuous transitions between the different dot magnetization states and perform excitation frequencies mapping. In any case it should not be excluded from consideration since the skyrmion or vortex metastable states have been demonstrated to be suitable for experimental study [38–40] and could be used in applications (e.g., in data storage [41]). Nanopatterning [42,43] might further increase a stability of such a metastable state [44].

The Néel-like skyrmion state is realized when $D > D_c(K_u)$, where the function $D_c(K_u)$ is defined by the line following yellow color in Fig. 2(b). The value of $D_c(K_u)$ decreases with K_u increasing, i.e., increase of K_u at $Q < 1$ leads to stabilization of the Néel skyrmion state. The further increase of the interface DMI parameter D or increase of the dot radius could lead to stabilization of cycloidal states that for very high values of the DMI strength were found as ground states in nanodots [35]. The intermediate states between the vortex and skyrmion are realized for intermediate values of the parameters. In this article we concentrate on the dynamical properties of the circular nanodot with values of the magnetic anisotropy constant and DMI strength that link the following four points and magnetic configurations indicated in Fig. 1: (i) $D = 0$, $K_u = 1.30 \times 10^6$ J/m^3—vortex state, (ii) $D = 0$, $K_u = 1.415 \times 10^6$ J/m^3—Bloch-like skyrmion, (iii) $D = 2 \times 10^{-3}$ J/m^2, $K_u = 1.415 \times 10^6$ J/m^3—Néel-like skyrmion with high quality factor Q, and (iv) $D = 2 \times 10^{-3}$ J/m^2, $K_u = 1.30 \times 10^6$ J/m^3—Néel-like skyrmion with low Q ($Q = 0.92$).

The magnetization vector dependence on the coordinates can be expressed in the polar coordinate system $\boldsymbol{m}(r,\phi)$ with the origin located in the dot center, see Fig. 1(i). Then the static and dynamical magnetization are expressed via their polar coordinate components m_ϕ, m_r, m_z and δm_ϕ, δm_r, δm_z, respectively. We express the magnetization components via the magnetization spherical angles Θ and Φ. For radially symmetric static magnetization configurations $\Theta = \Theta(r)$ and $\Phi = \Phi_0 + \phi$. The type of the skyrmion (Bloch-like or Néel-like) are distinguished with a function Φ_0 representing the skyrmion phase. It takes values $\pm\frac{\pi}{2}$ for the magnetic vortex or complete Bloch-like skyrmion (the in-plane magnetization is aligned along the azimuthal direction everywhere in the dot including the vortex/skyrmion edge) and $0,\pi$ for the complete Néel-like skyrmion (magnetization is along the radial direction). The different values of Φ_0 describe the vortex/skyrmion chirality and one of them should be chosen for a definite sign of the DMI parameter D. We define Φ_0 by using the magnetization orientation at the value of the radial coordinate equal to the skyrmion radius R_s [defined by the condition $m_z(r = R_s,\phi) = 0$]:

$$\Phi_0 = \arcsin\left(\frac{m_\phi}{\sqrt{m_r^2 + m_\phi^2}}\right). \tag{6}$$

The function Φ_0 over (D,K_u) plane is presented in Fig. 2(b). The general tendency is that the low values of DMI favor the Bloch-like skyrmion configuration (ii) and the high values of DMI are necessary to stabilize the Néel-like skyrmion (iii) and (iv). It is due to an interplay of the energy contributions that minimize the energy of Bloch-like or Néel-like skyrmions. When the DMI strength $D = 0$, the skyrmion magnetization profile is governed by the exchange, anisotropy, and magnetostatic energies, and the magnetization rotates in the dot plane perpendicular to the radial direction avoiding magnetostatic charges as $\nabla \cdot \boldsymbol{m} = 0$. The interface DMI introduces a contribution to the total energy that favors a spatially rotating magnetic state in a cycloidal mode with a nonzero m_ρ magnetization component. In thin films increasing DMI is sufficient to overcome the energy barrier forcing the transformation of the Bloch-like domain wall into the Néel-like wall [45,46]. We note that we consider the case of effective "easy plane" anisotropy $Q < 1$ and restricted in-plane geometry (circular dot). The vortex is stable when both (D,K_u) values are small. If $D = 0$ or small, a gradual increase of Q leads to transformation of the vortex state to the Bloch-like skyrmion state with $\Phi_0 = \pi/2$ avoiding an extra bulk and dot side surface magnetostatic energy. Increase of the interface DMI strength D for all considered values of Q results in a transition of these $\Phi_0 = \pi/2$ soliton states to a Néel-like skyrmion state with Φ_0 close to 0 or π to minimize the DMI energy. The transition is mainly determined by a competition of the interface DMI and volume/side surface magnetostatic energies because the isotropic exchange, magnetic anisotropy, and face magnetostatic energies are approximately the same for the vortex/Bloch-skyrmion and Néel-skyrmion states. The volume/side surface magnetostatic energies are proportional to the dot thickness t and, therefore, the transition takes place at relatively small values of $D = 0.7$–1.6×10^{-3} J/m^2 (Fig. 2), due to small dot thickness $t = 1.4$ nm.

Figure 2(c) shows the dependence of the skyrmion size R_s normalized to the dot radius R. Similarly to the phase Φ_0, the size of the skyrmion increases with the increase of the DMI strength and decreases with increase of the magnetic anisotropy constant K_u [10,47]. The Bloch-like skyrmion becomes unstable (R_s goes to zero) with respect to transition to the perpendicular single-domain state at Q approaching 1 and small $D < D_c(K_u) = 0.6 \times 10^{-3}$ J/m^3.

The analysis of Fig. 2 allows us to choose the path for study of the soliton dynamical excitations, where continuous transitions (second-order phase transition) happen: between the vortex and Bloch-like skyrmion along path (i) → (ii), between the Bloch-like skyrmion and Néel-like skyrmion with high Q along path (ii) → (iii), between high and low Q Néel-like skyrmions along the path (iii) → (iv), and finally between the Néel-like skyrmion and vortex state along path

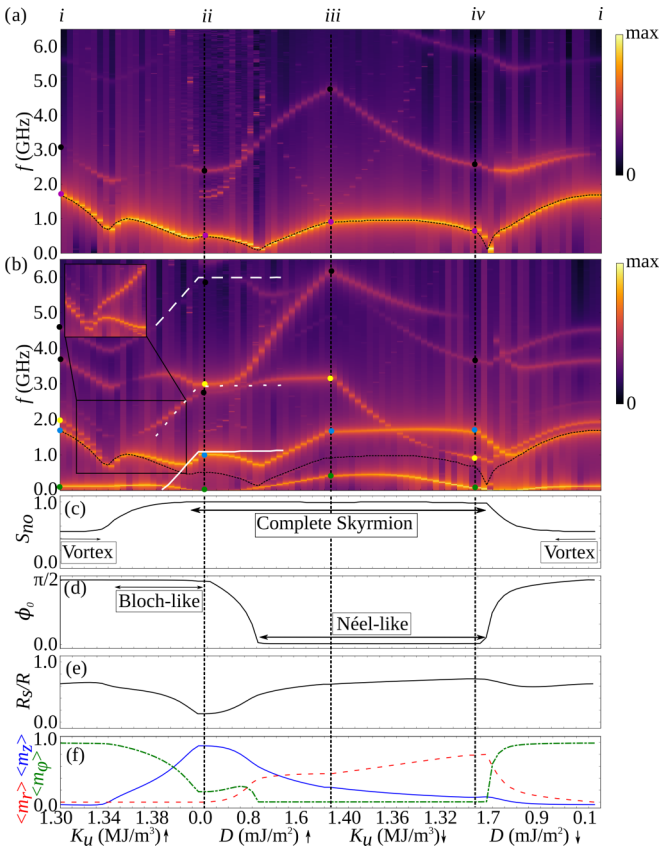

FIG. 3. The soliton resonance frequencies are plotted along the path presented in Fig. 2(a) between the four (i)–(iv) inhomogeneous magnetic configurations presented in Fig. 1. The frequency values are obtained with the spatially uniform microwave magnetic field excitation of the sinc type in time domain with (a) out-of-plane dynamic magnetization component and (b) in-plane magnetization component. The SW excitations in SD ground state are indicated with white solid, dotted, and dashed lines. The static properties of the solitons are presented by the skyrmion number (c) skyrmion number S_{no}, (d) skyrmion phase Φ_0, (e) skyrmion size R_s/R, and (f) the averaged magnetization components $\langle m_r \rangle$, $\langle m_\phi \rangle$, and $\langle m_z \rangle$ with red dashed, green dot-dashed, and blue continuous lines, respectively.

(iv) → (i). These paths are indicated in Fig. 2(a) with black straight arrows.

In the dynamical simulations there are spin eigenmodes keeping the radial symmetry of the soliton static state (radially symmetric or breathing modes) and the eigenmodes with broken radial symmetry [azimuthal modes rotating in the clockwise (CW) and counterclockwise (CCW) directions]. The radially symmetric modes have no net in-plane magnetization, and therefore, can be excited only by out-of-plane variable magnetic field. The azimuthal modes including gyrotropic ones can be excited by an in-plane variable magnetic field. The calculated frequencies of low-lying spin excitations along the defined above paths are presented in Fig. 3(a) for the out-of-plane excitation magnetic field and in Fig. 3(b) for the in-plane excitation magnetic field. The static properties presented in Fig. 2 are also plotted as a function of the dot magnetic parameters in Figs. 3(c)–3(f). The regions where soliton is in complete vortex, Bloch-like, Néel-like skyrmion, or in transition state can be clearly differentiated and are indicated in Figs. 3(c) and 3(d), and also in Fig. 2(a). Figure 3(f) demonstrates the second-order phase transitions, i.e., continuous transitions of the average magnetization components (the perpendicular $\langle m_z \rangle$, radial $\langle m_r \rangle$, and azimuthal $\langle m_\phi \rangle$ components) along the paths.

Additionally a frequency spectrum of the SW excitations in SD ground state are indicated with white solid, dotted, and dashed lines in Fig. 3(b). There are quasi-uniform and radial quantization modes that can be excited with uniform in-plane field [26]. In addition, a rich spectrum of azimuthal SW modes exist, but cannot be excited with uniform field [26,27]. Almost zero frequency of the quasi-uniform mode signals about a phase transition of the state at point near $K_u = 1.38 \times 10^6$ J/m^3 and $D = 0.0$ mJ/m^2. Such a transition was investigated in Ref. [27]. In contrast to the vortex to Bloch-like skyrmion transition or Bloch-like skyrmion to Néel-like skyrmion transition, continuity of the magnetization components and of the frequency spectrum is not preserved in the transition from the vortex to SD state.

Two main modes can be found in the excitation spectrum shown in Fig. 3(a) for the external microwave field perpendicular to the dot plane. The lowest frequency mode (purple dot and black dashed line) corresponds to the so called breathing skyrmion modes [20]. The higher frequency mode (marked by black dot) is a high order quantized mode of the same type of the radially symmetric excitations. Continuous transition of the mode frequencies along the path allows us to find corresponding modes in the vortex state, in the Bloch-like, and Néel-like skyrmions. The spatial profiles of the dynamic magnetization of the lowest frequency breathing mode for the four magnetic configurations (i)–(iv) are plotted in Fig. 4 (second column). For the vortex magnetic configuration $K_u = 1.3 \times 10^6$ J/m^3 and $D = 0$ mJ/m^2 (i) this mode can be characterized as an almost uniform radial mode. The SW amplitude is connected mainly with the radial magnetization component, that static configuration in a vortex state is close to 0 (see the first column in Fig. 4), and it oscillates in phase in a whole nanodot. With increase of the anisotropy the magnetic configuration is transformed to the Bloch-like skyrmion [point (ii)] and the character of the mode changes. The out-of-plane dynamic magnetization component is localized near the edge of skyrmion (near the skyrmion radius $r = R_s$), forms a ring around the skyrmion edge, and the magnetization oscillations are in phase. That is characteristic for the lowest breathing mode. Although the size of skyrmion is smallest among the considered configurations [Fig. 2(e)], the frequency of the breathing mode is quite low. With increasing D, its frequency still decreases up to transformation of the soliton into the Néel-like skyrmion, whereas the skyrmion radius increases. The breathing character of the mode and the area of the mode localization are preserved for the Néel-like skyrmion with high Q factor $K_u = 1.415 \times 10^6$ J/m^3 and $D = 2.0$ mJ/m^2 (iii) as well. Whereas for the Néel-like skyrmion with low Q factor, at point (iv) the amplitudes of the z and ϕ dynamical magnetization components are localized near the dot edge and the largest value of the static z-component amplitude is connected with the largest δm_ϕ component. This change might be attributed to the large size of the skyrmion and related edge effects or the large domain wall width

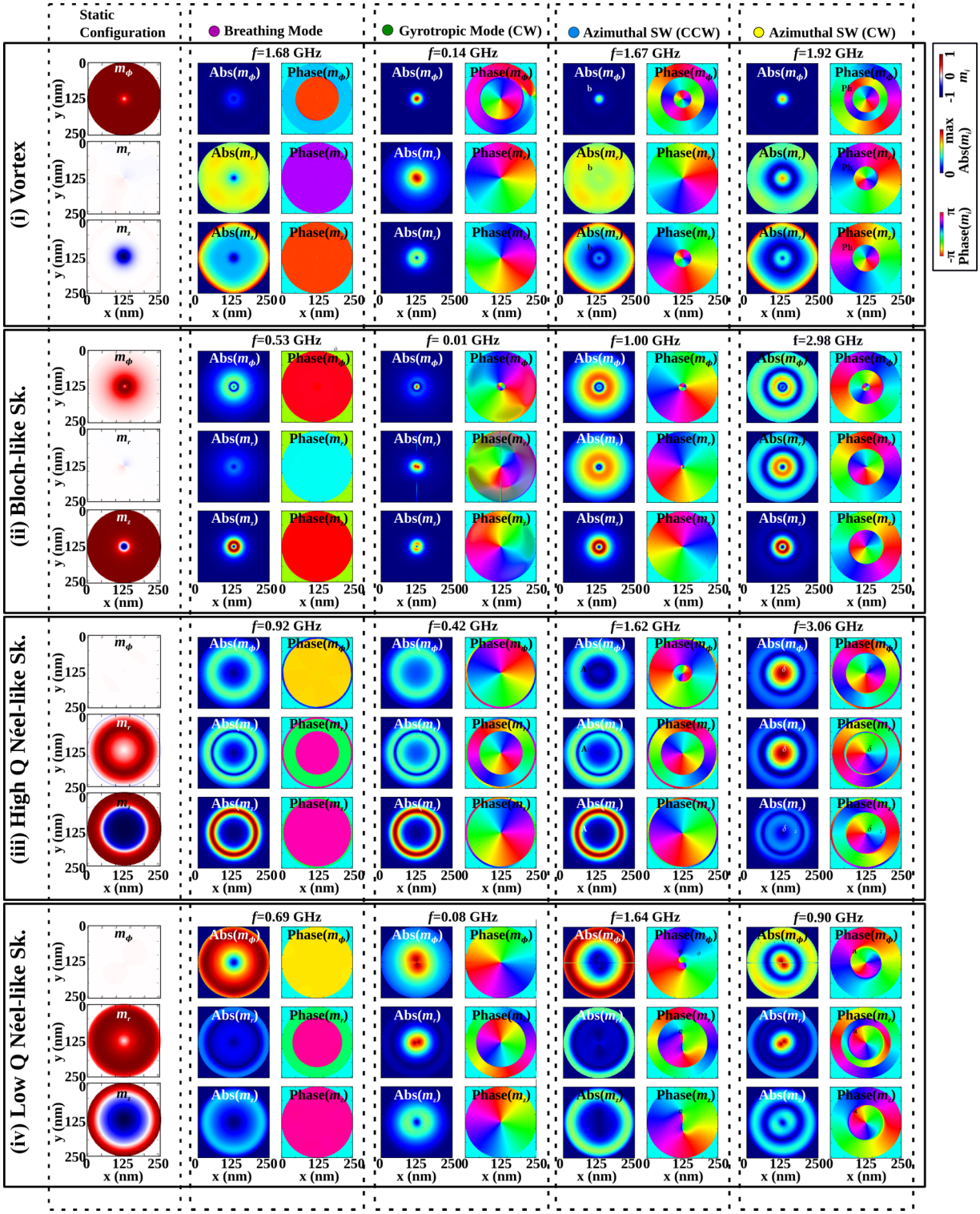

FIG. 4. The static (first column in the left) and dynamic magnetization components δm_ϕ, δm_r and δm_z of the isolated circular dot in the soliton magnetic configurations: vortex (i), Bloch-like (ii), and Néel-like (iii) and (iv) skyrmions. The respective magnetic configurations are presented in Fig. 1, the resonance frequencies are indicated as grid vertical line in Figs. 3(a) and 3(b).

related to the low value of Q factor [48,49]. Interestingly, the frequency of the breathing mode has a local minimum at every transformation of the magnetization configuration (between the vortex and Bloch-like skyrmion, Bloch-like and Néel-like skyrmion, and Néel-like skyrmion and the vortex), while it is weakly dependent on the changes of quality factor Q for the Néel-like skyrmion. The local minima or maxima of the spin mode frequency mode might signal about an onset of the change of the soliton character. Thus, the deep local minima correspond to the onsets in the change of the $\langle m_r \rangle$, $\langle m_\phi \rangle$, and $\langle m_z \rangle$ functions. In other words, when the changes in $\langle m_r \rangle$, $\langle m_\phi \rangle$, and $\langle m_z \rangle$ have small gradient, the changes of the

soliton shape are also small, and the monotonous behavior of frequency can be observed with change of D or K_u. If a large gradient is present in the functions $\langle m_r \rangle$, $\langle m_\phi \rangle$, and $\langle m_z \rangle$ in dependence on D or K_u, then the shape of the soliton is altered and due to this, the nonmonotonous change in frequency of the breathing mode is observed. Additionally, the vanishing frequency might be signaling about a border of the soliton stability or degeneracy of the stable configuration.

Figure 3(b) represents the soliton eigenfrequencies when the driving magnetic field is in-plane of the dot. Due to the symmetry of the breathing mode, it cannot be excited effectively with such a field. Instead, other modes are visible in the dot excitation spectrum. Here we concentrate on three low-frequency excitation modes that correspond to gyrotropic mode and CCW, CW azimuthal SW modes. The modes are indicated with green, blue, and yellow dots, respectively.

The lowest frequency mode is a gyrotropic excitation directly related to the soliton topological charge given by Eq. (5). This mode is a precession of the vortex/skyrmion core around its equilibrium position in the dot center (CW for the given soliton core polarization $p = -1$). It is characterized with the out-of-plane dynamic magnetization component (m_z) localized near the edge of the soliton for all considered inhomogeneous dot magnetization configurations. The mode amplitude forms a ring around the soliton edge (see Fig. 4, the column in the middle). The magnetization oscillations are not in-phase around the dot, the phase changes continuously from $-\pi$ to π. This character is preserved for all magnetization configurations apart from the Néel-like skyrmion with low Q factor, where due to large size of the skyrmion, the nanodot edge effects, or considerable domain wall width provide changes in the amplitude localization of the m_z magnetization component of this mode. Due to the skyrmion size is comparable with the dot radius, the maximum amplitude of m_z is pushed toward the dot center, the ring is not formed at the skyrmion edge, but inside the skyrmion core instead. The anomalies of phase of the gyrotropic mode for the Bloch-like skyrmion are present in the area where $\mathrm{Abs}(m_i)$ is close to zero and the intensity of SW is too low for correct definition of the phase. The in-plane dynamical magnetization components are also concentrated near the skyrmion radius except the case of Néel-like skyrmion (iv), where they are localized at the dot center.

Two dynamic magnetization components in the local coordinate system with Oz' axis directed along the skyrmion static magnetization $\mathbf{m}(\Theta, \Phi)$ can be represented as

$$a_n(r)\cos(m\phi - \omega t + \phi_0), \quad b_n(r)\sin(m\phi - \omega t + \phi_0),$$

where a_n, b_n are the SW mode radial profiles, n is number of nodes along radial direction (radial mode index), m is the azimuthal mode index, and ϕ_0 is a constant. The soliton dynamical magnetization components δm_r, δm_ϕ, δm_z can be represented as linear combination of these two magnetization components involving the skyrmion static magnetization angles Θ and Φ_0.

Accordingly, the CW gyrotropic mode can be described by the azimuthal index $m = -1$. The gyrotropic mode possesses a finite frequency in the sub-GHz range for the whole studied range of parameters with two minima and is close to zero frequency for the Bloch-like skyrmion [around (ii)] and the Néel-like skyrmion with low Q factor [near (iv)]. The vanishing frequency is a characteristic property of the gyrotropic mode signaling about a border of the soliton stability. The gyrotropic mode softening was also simulated near the transition of the vortex state to the saturated state of the circular dots increasing out-of-plane magnetic field, when the gyrotropic mode transforms into the quasi-uniform Kittel mode [27]. The minimum of frequency corresponds to two magnetization configurations with smallest (ii) and largest (iv) skyrmion radius, the inhomogeneous magnetization states closest to the uniform state.

Two remaining excitation modes in the vortex state are the modes corresponding to the CCW ($m = +1$) and CW ($m = -1$) SW azimuthal modes (see the mode profiles in Fig. 4 in the last two columns). If the vortex core is neglected, they have no radial nodes, thus $n = 0$ [50]. In a vortex state (i) the degeneracy of the CW and CCW spin waves is lifted due to the dynamic hybridization of the azimuthal SWs with the gyrotropic mode [8]. This hybridization is especially strong for the $m = -1$ SW mode and small dot radius R resulting in formation of a radial node near the vortex core edge. We note that the dots of small radius R about of 100 nm are of special interest for the magnetic skyrmion stabilization and the skyrmion radius can be large, comparable with the dot radius, and it cannot be neglected anymore. Therefore, the classification of the low-lying SW modes by the indices $m = +1, n = 0$ (CCW) and $m = -1, n = 1$ (CW) seems to be more adequate. It is applicable to describe the low-frequency SW modes of the vortex, Bloch-skyrmion (except the limiting case $Q \to 0$), and Néel-skyrmion (iii) states, see Fig. 4. The mode frequencies decrease with increasing K_u when the magnetic stable state is vortex. During transition from the vortex to the Bloch-like skyrmion, the spatial distribution of the CW spin-wave mode changes. The mode localization area is transferred from the edge to the dot center and at certain values of the magnetic anisotropy K_u close to the point $Q = 1$ the mode cannot be effectively excited with an in-plane variable magnetic field. To check whether the separation of the CW and CCW modes are preserved in the transition point we have repeated simulations but with the point excitation (100 nm diameter circle localized at center of the nanodot). Indeed, these modes are split as it is shown in the inset in Fig. 3 in the transition point. With further increase of the anisotropy constant the Bloch-like skyrmion forms and the frequency separation between CW and CCW modes increases significantly. Therefore, the CCW ($m = +1$, $n = 1$) SW becomes third mode in the excitation spectrum. Such mode frequencies inversion is related to the localization of these modes in the skyrmion state, which is different from one in the vortex state, where the vortex core occupies a small area of the dot. The frequency inversion is accompanied with strong hybridization and inversion in the sense of propagation of the CW ($m = -1$, $n = 1$) mode. In the skyrmion states we can distinguish azimuthal SW modes as center localized or edge localized SWs. With transformation of the magnetization configuration between different skyrmion states this particularity is preserved and mostly pronounced among the skyrmion states in state (iii) where a strong localization of the azimuthal SW is present at the skyrmion center (fifth column in Fig. 4) or skyrmion edge (fourth column). Nevertheless, the origin of this frequency splitting

is not clear at this moment and the gyrotropic mode can contribute to this [22].

In the case of Néel-like skyrmion configuration with high Q factor (iii), the lower frequency azimuthal SW could be also interpreted as a CCW gyrotropic mode [14] and in fact there is a big resemblance of the dynamic components of the magnetization vector. Nevertheless, the origin of this mode is due to azimuthal SW excitation over the skyrmion background and the difference between the gyrotropic mode and lowest azimuthal SW mode is pronounced when the size of the skyrmion is much smaller than the dot size. The localization area of the in-plane magnetization components of the azimuthal SW mode spreads within the dot and the in-plane magnetization components of the gyrotropic mode are localized near the skyrmion edge (ii). Another difference is the link of the gyrotropic mode sense of rotation with the sign of the topological charge or gyrovector ($p = +1/-1$). With respect to the CW and CCW SW mode frequencies splitting, it is also interesting the variation of these modes with decreasing K_u in the Néel-like skyrmion [on the path between (iii) and (iv) states], where the frequency order of these modes changes, without any signature of their interaction at their frequencies crossing [Fig. 3(b)]. In the Néel-skyrmion state (iv) the spin excitation spectrum is consequence of the CW gyrotropic ($m = -1$), CW SW ($m = -1, n = 1$), and CCW SW ($m = +1, n = 0$) modes. Whereas the consequence for the vortex, Bloch- (ii), and Néel-skyrmion (iii) states is the following: CW gyrotropic ($m = -1$), CCW SW ($m = +1, n = 0$), and CW SW ($m = -1, n = 1$) modes. Another peculiarity of the Néel-skyrmion (iv) state is strong localization of the high frequency CCW SW mode near the dot edge.

We note also that there is a correspondence between azimuthal CCW spin-wave mode $m = +1, n = 0$ (blue dots) and uniform radial mode $m = 0, n = 0$ (purple dots) in the dynamical magnetization spatial distribution and the frequency dependence on the parameters D, K_u for all inhomogeneous magnetic configurations considered. This similarity is indicated in Figs. 3(a) and 3(b) by the dashed black line.

IV. SUMMARY

We have determined the spin excitation spectra of a circular magnetic dot in four topologically nontrivial inhomogeneous magnetization states, and showed the continuous transitions between them. Using spin-wave eigenmode mapping we have elucidated the origin of the spin excitations on the skyrmion background and proposed a spin mode classification similar to that developed for the spin excitations in the magnetic vortex state circular dots (with $K_u = 0$) based on the azimuthal and radial mode indices (m,n). The excitation spectrum on the vortex background with large K_u is similar to that of the vortex state in a soft magnetic dot in that it has a low-frequency gyrotropic mode, an $m = +1/-1$ azimuthal mode doublet, and a radial mode $(m = 0, n = 0)$ with approximately the same frequencies. In the skyrmion state the radial mode frequency is essentially lower than the azimuthal SW frequencies and the frequency splitting between the azimuthal ($m = +1$ and $m = -1$) spin-wave modes is essentially larger than one in a vortex state dot.

ACKNOWLEDGMENTS

One of the co-authors (K.G.) thanks B. A. Ivanov for discussions of the magnetic soliton dynamics. The project is financed from the SASPRO Programme. The research has received funding from the People Programme (Marie Curie Actions) European Union's Seventh Framework Programme under REA Grant Agreement No. 609427 (Project WEST: 1244/02/01). The research has been further co-funded by the Slovak Academy of Sciences and the European Union Horizon 2020 Research and Innovation Programme under Marie Sklodowska-Curie Grant Agreement No. 644348 (MagIC). K.G. acknowledges support by IKERBASQUE (the Basque Foundation for Science), the Spanish MINECO Grant No. MAT2013-47078-C2-1-P and the Spanish MINECO Grant No. FIS2016-78591-C3-3-R. The numerical calculations were partially performed at the Poznan Supercomputing and Networking Center (Grant No. 209).

[1] A. M. Kosevich, B. Ivanov, and A. Kovalev, Phys. Rep. **194**, 117 (1990).
[2] T. Shinjo, T. Okuno, R. Hassdorf, K. Shigeto, and T. Ono, Science **289**, 930 (2000).
[3] K. Y. Guslienko, B. Ivanov, V. Novosad, Y. Otani, H. Shima, and K. Fukamichi, J. Appl. Phys. **91**, 8037 (2002).
[4] K. Y. Guslienko, X. F. Han, D. J. Keavney, R. Divan, and S. D. Bader, Phys. Rev. Lett. **96**, 067205 (2006).
[5] J. P. Park and P. A. Crowell, Phys. Rev. Lett. **95**, 167201 (2005).
[6] S. Mamica, J. S. Lévy, and M. Krawczyk, J. Phys. D **47**, 015003 (2013).
[7] K. Y. Guslienko, V. Novosad, Y. Otani, H. Shima, and K. Fukamichi, Phys. Rev. B **65**, 024414 (2001).
[8] K. Y. Guslienko, A. N. Slavin, V. Tiberkevich, and S.-K. Kim, Phys. Rev. Lett. **101**, 247203 (2008).
[9] B. Pigeau, G. De Loubens, O. Klein, A. Riegler, F. Lochner, G. Schmidt, L. Molenkamp, V. Tiberkevich, and A. Slavin, Appl. Phys. Lett. **96**, 132506 (2010).
[10] C. Moreau-Luchaire, C. Moutafis, N. Reyren, J. Sampaio, C. Vaz, N. Van Horne, K. Bouzehouane, K. Garcia, C. Deranlot, P. Warnicke *et al.*, Nat. Nanotechnol. **11**, 444 (2016).
[11] O. Boulle, J. Vogel, H. Yang, S. Pizzini, D. de Souza Chaves, A. Locatelli, T. O. Menteş, A. Sala, L. D. Buda-Prejbeanu, O. Klein *et al.*, Nat. Nanotechnol. **11**, 449 (2016).
[12] S. Woo, K. Litzius, B. Krüger, M.-Y. Im, L. Caretta, K. Richter, M. Mann, A. Krone, R. M. Reeve, M. Weigand *et al.*, Nat. Mater. **15**, 501 (2016).
[13] F. Büttner, C. Moutafis, M. Schneider, B. Krüger, C. Günther, J. Geilhufe, C. v. K. Schmising, J. Mohanty, B. Pfau, S. Schaffert *et al.*, Nat. Phys. **11**, 225 (2015).
[14] M. Mochizuki, Phys. Rev. Lett. **108**, 017601 (2012).
[15] Y. Okamura, F. Kagawa, M. Mochizuki, M. Kubota, S. Seki, S. Ishiwata, M. Kawasaki, Y. Onose, and Y. Tokura, Nat. Commun. **4**, 2391 (2013).
[16] T. Schwarze, J. Waizner, M. Garst, A. Bauer, I. Stasinopoulos, H. Berger, C. Pfleiderer, and D. Grundler, Nat. Mater. **14**, 478 (2015).

[17] J. Sampaio, V. Cros, S. Rohart, A. Thiaville, and A. Fert, Nat. Nanotechnol. **8**, 839 (2013).
[18] B. A. Ivanov, V. Muravev, and D. D. Sheka, J. Exp. Theor. Phys. **89**, 583 (1999).
[19] D. D. Sheka, B. A. Ivanov, and F. G. Mertens, Phys. Rev. B **64**, 024432 (2001).
[20] J. V. Kim, F. Garcia-Sanchez, J. Sampaio, C. Moreau-Luchaire, V. Cros, and A. Fert, Phys. Rev. B **90**, 064410 (2014).
[21] J. Iwasaki, M. Mochizuki, and N. Nagaosa, Nat. Nanotechnol. **8**, 742 (2013).
[22] Z. V. Gareeva and K. Y. Guslienko, Phys. Status Solidi Rapid Res. Lett. **10**, 227 (2016).
[23] K. Y. Guslienko and Z. V. Gareeva, IEEE Magn. Lett. **8**, 4100305 (2017).
[24] M. Mruczkiewicz, P. Gruszecki, M. Zelent, and M. Krawczyk, Phys. Rev. B **93**, 174429 (2016).
[25] I. Makhfudz, B. Krüger, and O. Tchernyshyov, Phys. Rev. Lett. **109**, 217201 (2012).
[26] V. Castel, J. Ben Youssef, F. Boust, R. Weil, B. Pigeau, G. de Loubens, V. V. Naletov, O. Klein, and N. Vukadinovic, Phys. Rev. B **85**, 184419 (2012).
[27] B. Taurel, T. Valet, V. V. Naletov, N. Vukadinovic, G. de Loubens, and O. Klein, Phys. Rev. B **93**, 184427 (2016).
[28] A. Vansteenkiste, J. Leliaert, M. Dvornik, M. Helsen, F. Garcia-Sanchez, and B. Van Waeyenberge, AIP Adv. **4**, 107133 (2014).
[29] A. N. Bogdanov and U. K. Rößler, Phys. Rev. Lett. **87**, 037203 (2001).
[30] The cell size below 1 nm was used, $\frac{250\times10^{-9}}{256}$. The maximum amplitude of the sinc signal was $I = 0.0001$ T and it was positioned at 1 ns after the start of simulations.
[31] The rectangular window function was used in the Fourier transform with 50 ns width, starting 4 ns after the peak of the sinc signal, providing 20 MHz frequency resolution, $\Delta f = 20$ MHz.
[32] Y. Nakatani, M. Hayashi, S. Kanai, S. Fukami, and H. Ohno, Appl. Phys. Lett. **108**, 152403 (2016).
[33] A. Natarajarathinam, Z. R. Tadisina, T. Mewes, S. Watts, E. Chen, and S. Gupta, J. Appl. Phys. **112**, 053909 (2012).
[34] H. Yu, R. Huber, T. Schwarze, F. Brandl, T. Rapp, P. Berberich, G. Duerr, and D. Grundler, Appl. Phys. Lett. **100**, 262412 (2012).
[35] J. Mulkers, M. V. Milošević, and B. Van Waeyenberge, Phys. Rev. B **93**, 214405 (2016).
[36] N. Nagaosa and Y. Tokura, Nat. Nanotechnol. **8**, 899 (2013).
[37] C. Heo, N. S. Kiselev, A. K. Nandy, S. Blügel, and T. Rasing, Sci. Rep. **6**, 27146 (2016).
[38] H. Oike, A. Kikkawa, N. Kanazawa, Y. Taguchi, M. Kawasaki, Y. Tokura, and F. Kagawa, Nat. Phys. **12**, 62 (2016).
[39] K. S. Buchanan, P. E. Roy, M. Grimsditch, F. Y. Fradin, K. Y. Guslienko, S. D. Bader, and V. Novosad, Nat. Phys. **1**, 172 (2005).
[40] G. de Loubens, A. Riegler, B. Pigeau, F. Lochner, F. Boust, K. Y. Guslienko, H. Hurdequint, L. W. Molenkamp, G. Schmidt, A. N. Slavin, V. S. Tiberkevich, N. Vukadinovic, and O. Klein, Phys. Rev. Lett. **102**, 177602 (2009).
[41] C. A. Ross and F. J. Castano, Magnetic memory elements using 360° walls, US Patent 6,906,369, 2005.
[42] Y. Y. Dai, H. Wang, P. Tao, T. Yang, W. J. Ren, and Z. D. Zhang, Phys. Rev. B **88**, 054403 (2013).
[43] D. A. Gilbert, B. B. Maranville, A. L. Balk, B. J. Kirby, P. Fischer, D. T. Pierce, J. Unguris, J. A. Borchers, and K. Liu, Nat. Commun. **6**, 8462 (2015).
[44] An estimation of the barrier between the metastable Bloch skyrmion and perpendicular SD states has been made using the semianalytic calculations within a radially symmetric Bloch-like skyrmion ansatz. The value of the barrier E is approximately $0.01 M_S^2 V$ (V is the dot volume). The ratio $\frac{E}{(k_B T)}$ is about 37–38 at room temperature that corresponds to the relaxation time about of 6 months for our dot parameters (we assumed that the Néel-Arrhenius law is valid and the attempt time is 1 ns).
[45] A. Thiaville, S. Rohart, É. Jué, V. Cros, and A. Fert, Europhys. Lett. **100**, 57002 (2012).
[46] M. Heide, G. Bihlmayer, and S. Blügel, Phys. Rev. B **78**, 140403 (2008).
[47] K. Y. Guslienko, IEEE Magn. Lett. **6**, 4000104 (2015).
[48] M. Kisielewski, A. Maziewski, V. Zablotskii, T. Polyakova, J. Garcia, A. Wawro, and L. Baczewski, J. Appl. Phys. **93**, 6966 (2003).
[49] F. Virot, L. Favre, R. Hayn, and M. Kuz'min, J. Phys. D **45**, 405003 (2012).
[50] K. Y. Guslienko, G. R. Aranda, and J. M. Gonzalez, Phys. Rev. B **81**, 014414 (2010).